International Journal of Modern Physics B
Vol. 29, No. 28 (2015) 1550194 (19 pages)

DOI: 10.1142/S0217979215501945

World Scientific
www.worldscientific.com

Critical behaviors and phase diagrams of the mixed spin-1 and spin-7/2 Blume-Capel (BC) Ising model on the Bethe lattice (BL)

M. Karimou*, R. Yessoufou*,†,‡ and F. Hontinfinde*,†

*Institute of Mathematics and Physical Sciences (IMSP), Dangbo, Porto-Novo, BP 526, Abomey-Calavi, 229 Littoral, Contonou, Republic of Benin
†Department of Physics, University of Abomey-Calavi, Republic of Benin
‡yesradca@yahoo.fr

Received 26 April 2015
Revised 31 July 2015
Accepted 3 August 2015
Published 1 October 2015

Using the recursion equations technique, the influences of the single-ion anisotropies or crystal-fields interactions on the magnetic properties of the mixed spin-1 and spin-7/2 Blume-Capel (BC) Ising ferrimagnetic system are studied on the Bethe lattice (BL). The ground-state phase diagram is constructed, the thermal behaviors of the order-parameters and the free-energy are thoroughly investigated in order to characterize the nature of the phase transitions and to obtain the phase transition temperature. Then, the temperature phase diagrams are obtained in the case of equal crystal-field interactions on the ($kT/|J|$ and $D/|J|$) planes when $q = 3, 4$ and 6 and in the case of unequal crystal-fields interactions on the ($kT/|J|$ and $D_A/|J|$) and ($kT/|J|$ and $D_B/|J|$) planes for selected values of $D_B/|J|$ and $D_A/|J|$ respectively when $q = 3$. The model shows first-order and second-order phase transitions, and where the lines are connected is the tricritical point. Besides the first-order and second-order phase transitions, the system also exhibits compensation temperatures depending on appropriate values of the crystal-fields interactions.

Keywords: BC model; Bethe lattice; ferrimagnetic; ground-state phase diagram; tricritical point.

PACS numbers: 05.50.+q, 05.70.Ce, 64.60.Cn, 75.10.Hk, 75.30.Gw

1. Introduction

In the last five decades, the Ising model has been one of the most largely used models to describe critical behaviors of several systems in nature. Recently,

‡Corresponding author.

several extensions have been made in the spin-1/2 Ising model to describe a wide variety of systems. For example, the models consisting of mixed-spins with different magnitudes are interesting extensions, forming the so-called mixed-spin Ising class. Beyond that, magnetic materials have numerous and important technological applications: They find wide use in information storage devices, microwaves communications systems, electric power transformers and dynamo and high-fidelity speakers.[1–4] Thus, in response to the increasing demands being placed on the performance of magnetic solids, there has been a surge of interest in molecular-based magnetic materials.[5–8] Indeed, the discovery of these materials[9] has been one of the advances in modern magnetism. Many magnetic materials have two types of magnetic atoms regularly alternating which exhibit ferrimagnetism. In this context, a good description of their physical properties is given by means of mixed-spin configurations. The interest in studying magnetic properties of these materials is due to their reduced translational symmetry rather than to their single-spin counterparts, since they consist of two interpenetrating sublattices. Thus, ferrimagnetic materials are of great interest due to their possible technological applications and from a fundamental point of view. These materials are modeled by mixed-spin Ising models that can be built up by infinite combinations of different spins, where the pairs constituted by spins with small values are the simplest: $(1/2, 1)$, $(1/2, 3/2)$, $(1, 3/2)$, $(1, 5/2)$, $(2, 3/2)$, $(2, 5/2)$ and so on.

There are many studies on mixed-spin Ising systems aiming to explain the physical properties of disordered systems. In this regard, there has been great interest in the study of magnetic properties of systems formed by two sublattices with different spins and crystal-fields interactions.[10] Theoretically, such systems have been widely studied by a variety of methods e.g., effective-field theory,[11–20] mean-field approximation,[21–23] renormalization-group technique,[24] numerical simulations based on Monte Carlo[25–34] and exact recursion equations.[35–37] A more recent interest is to extend such investigations into a more general mixed-spin Ising model with one constituent spin-1 and the other constituent spin-7/2. In this context, Hadey[38] presented a mean-field theory based on the Bogoliubov inequality for Gibbs free-energy study to elucidate only crystal-fields and longitudinal field effects on the thermodynamic quantities particularly on the existence and induction of compensation temperatures.

In this paper, we adopt the exact recursion equations technique for the study of temperature phase diagrams of the mixed spin-1 and spin-7/2 Blume-Capel (BC) Ising model with two different crystal-fields on the Bethe lattice (BL). The purpose of this work is to clarify the influences of the two crystal-fields on the physical properties of the model.

The outline of this work is arranged as follows. In Sec. 2, the formulation of the model on the BL is specified and all the thermodynamical quantities of interest are calculated in terms of recursion relations. In the next section, a brief definition of the critical temperatures of the model is given. The illustrations and discussions

of the numerical results are presented in Sec. 4. The last section is devoted to the conclusion.

2. Description of the Model on the Bethe Lattice

The mixed-spins system on the BL is shown in Fig. 1. We consider the mixed spin-1 and spin-7/2 system consisting of two sublattices A and B. The sites of sublattice A are occupied by atoms of spins S_i, where $S_i = \pm 1$ and 0. Those of the sublattice B are occupied by atoms of spins σ_j, where $\sigma_j = \pm(7/2), \pm(5/2), \pm(3/2)$ and $\pm(1/2)$. In our case, the BL is arranged such that the central spin is spin-1 and the next generation spin is spin-7/2 and so on to infinity. Thus, the Ising Hamiltonian of such model on the BL may be written as

$$H = -J \sum_{\langle i,j \rangle} \sigma_j S_i - D_A \sum_i S_i^2 - D_B \sum_j \sigma_j^2 \,, \tag{1}$$

$J < 0$ is the bilinear exchange coupling interaction strength. D_A and D_B are the single-ion anisotropies or the crystal-fields acting on spins of sublattices A and B respectively.

In order to formulate the problem on the BL, the partition function is the main ingredient which is given as

$$Z = \sum e^{-\beta H} = \sum \exp \left[\beta \left(J \sum_{\langle i,j \rangle} \sigma_j S_i + D_A \sum_i S_i^2 + D_B \sum_j \sigma_j^2 \right) \right] . \tag{2}$$

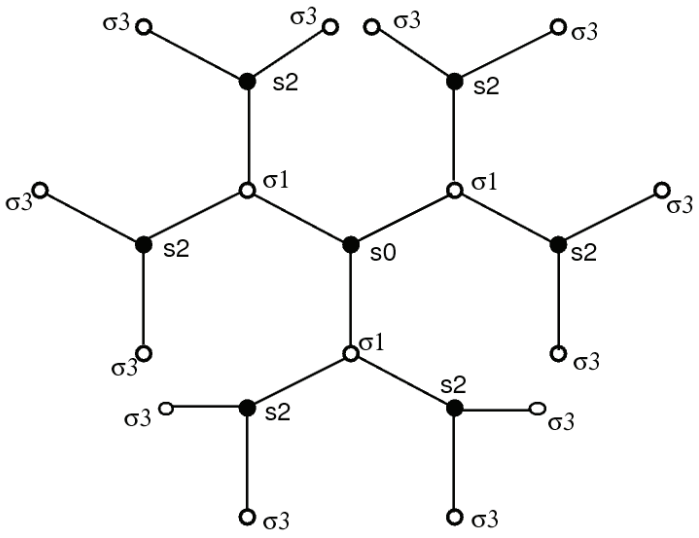

Fig. 1. The mixed-spin Ising model consisting of two different magnetic atoms with spins values $s_i = 1$ and $\sigma_j = 7/2$ respectively defined on the BL with coordination number $q = 3$.

If the BL is cut at the central spin S_0, it splits into q disconnected pieces. So, the partition function on the BL can be written as

$$Z = \sum_{S_0} \exp(\beta D_A S_0^2) g_n^q(S_0)\,, \tag{3}$$

where S_0 is the central spin value of the lattice, $g_n(S_0)$ the partition function of an individual branch and the suffix n represents the fact that the sub-tree has n shells, i.e., n steps from the root to the boundary sites. If we continue to cut the BL on the sites σ_1 and S_2 which are respectively the nearest and next nearest of the central spin S_0, we can obtain the recurrence relations for $g_n(S_0)$ and $g_{n-1}(\sigma_1)$ as

$$g_n(S_0) = \sum_{\{\sigma_1\}} \exp[\beta(JS_0\sigma_1 + D_B\sigma_1^2)][g_{n-1}(\sigma_1))]^{q-1}\,, \tag{4}$$

$$g_{n-1}(\sigma_1) = \sum_{\{S_2\}} \exp[\beta(JS_2\sigma_1 + D_A S_2^2)][g_{n-2}(S_2))]^{q-1}\,. \tag{5}$$

Now, we can explicitly calculate for example, some $g_n(S_0)$ and $g_{n-1}(\sigma_1)$ given by

$$\begin{aligned}
g_n(\pm 1) &= \sum_{\{\sigma_1\}} \exp[\beta(\pm J\sigma_1 + D_B\sigma_1^2)][g_{n-1}(\sigma_1))]^{q-1} \\
&= e^{\beta(\pm\frac{7J}{2}+\frac{49}{4}D_B)}\left[g_{n-1}\left(\frac{7}{2}\right)\right]^{q-1} + e^{\beta(\mp\frac{7J}{2}+\frac{49}{4}D_B)}\left[g_{n-1}\left(\frac{-7}{2}\right)\right]^{q-1} \\
&\quad + e^{\beta(\pm\frac{5J}{2}+\frac{25}{4}D_B)}\left[g_{n-1}\left(\frac{5}{2}\right)\right]^{q-1} + e^{\beta(\mp\frac{5J}{2}+\frac{25}{4}D_B)}\left[g_{n-1}\left(\frac{-5}{2}\right)\right]^{q-1} \\
&\quad + e^{\beta(\pm\frac{3J}{2}+\frac{9}{4}D_B)}\left[g_{n-1}\left(\frac{3}{2}\right)\right]^{q-1} + e^{\beta(\mp\frac{3J}{2}+\frac{9}{4}D_B)}\left[g_{n-1}\left(\frac{-3}{2}\right)\right]^{q-1} \\
&\quad + e^{\beta(\pm\frac{J}{2}+\frac{1}{4}D_B)}\left[g_{n-1}\left(\frac{1}{2}\right)\right]^{q-1} + e^{\beta(\mp\frac{J}{2}+\frac{1}{4}D_B)}\left[g_{n-1}\left(\frac{-1}{2}\right)\right]^{q-1}\,,
\end{aligned} \tag{6}$$

$$\begin{aligned}
g_{n-1}\left(\pm\frac{7}{2}\right) &= \sum_{\{S_2\}} \exp\left[\beta\left(\frac{\pm 7J}{2}S_2 + D_A S_2^2\right)\right][g_{n-2}(S_2))]^{q-1} \\
&= e^{\beta(\pm\frac{7J}{2}+D_A)}[g_{n-2}(1)]^{q-1} + e^{\beta(\mp\frac{7J}{2}+D_A)}[g_{n-2}(-1)]^{q-1} + g_{n-2}^{q-1}(0).
\end{aligned} \tag{7}$$

After calculating all the $g_n(S_0)$ and $g_{n-1}(\sigma_1)$, we can define the recursion relations for the spin-1 as

$$Y_n = \frac{g_n(+1)}{g_n(0)}\,, \quad Z_n = \frac{g_n(-1)}{g_n(0)} \tag{8}$$

and for the spin-7/2 as

$$A_{n-1} = \frac{g_{n-1}\left(\frac{+7}{2}\right)}{g_{n-1}\left(\frac{-1}{2}\right)}, \quad B_{n-1} = \frac{g_{n-1}\left(\frac{-7}{2}\right)}{g_{n-1}\left(\frac{-1}{2}\right)},$$
$$C_{n-1} = \frac{g_{n-1}\left(\frac{+5}{2}\right)}{g_{n-1}\left(\frac{-1}{2}\right)}, \quad D_{n-1} = \frac{g_{n-1}\left(\frac{-5}{2}\right)}{g_{n-1}\left(\frac{-1}{2}\right)},$$
$$E_{n-1} = \frac{g_{n-1}\left(\frac{3}{2}\right)}{g_{n-1}\left(\frac{-1}{2}\right)}, \quad F_{n-1} = \frac{g_{n-1}\left(\frac{-3}{2}\right)}{g_{n-1}\left(\frac{-1}{2}\right)},$$
$$G_{n-1} = \frac{g_{n-1}\left(\frac{+1}{2}\right)}{g_{n-1}\left(\frac{-1}{2}\right)}. \tag{9}$$

To investigate our model, we define two order-parameters, the magnetization M and the corresponding quadrupolar moment Q. For the sublattice A, the order-parameters are respectively defined by

$$M_A = Z_A^{-1} \sum_{\{S_0\}} S_0 \exp(\beta D_A S_0^2) g_n^q(S_0),$$
$$Q_A = Z_A^{-1} \sum_{\{S_0\}} S_0^2 \exp(\beta D_A S_0^2) g_n^q(S_0). \tag{10}$$

After some mathematical calculations, the two order-parameters are expicitly calculated as:

$$M_A = \frac{e^{(\beta D_A)}(Y_n^q - Z_n^q)}{e^{(\beta D_A)}(Y_n^q + Z_n^q) + 1}, \tag{11}$$

$$Q_A = \frac{e^{(\beta D_A)}(Y_n^q + Z_n^q)}{e^{(\beta D_A)}(Y_n^q + Z_n^q) + 1}. \tag{12}$$

In the same way, we also calculate the two order-parameters for the sublattice B as follows:

$$M_B = \frac{M'_B}{M_B^0}, \quad Q_B = \frac{Q'_B}{Q_B^0}.$$

where

$$M'_B = 7e^{(\frac{49}{4}\beta D_B)}(A_{n-1}^q - B_{n-1}^q) + 5e^{(\frac{25}{4}\beta D_B)}(C_{n-1}^q - D_{n-1}^q)$$
$$+ 3e^{(\frac{9}{4}\beta D_B)}(E_{n-1}^q - F_{n-1}^q) + e^{(\frac{1}{4}\beta D_B)}(G_{n-1}^q - 1), \tag{13}$$

$$M_B^0 = 2e^{(\frac{49}{4}\beta D_B)}(A_{n-1}^q + B_{n-1}^q) + 2e^{(\frac{25}{4}\beta D_B)}(C_{n-1}^q + D_{n-1}^q) + 2e^{(\frac{9}{4}\beta D_B)}(E_{n-1}^q + F_{n-1}^q) + 2e^{(\frac{1}{4}\beta D_B)}(G_{n-1}^q + 1)\,, \tag{14}$$

$$Q_B' = 49e^{(\frac{49}{4}\beta D_B)}(A_{n-1}^q + B_{n-1}^q) + 25e^{(\frac{25}{4}\beta D_B)}(C_{n-1}^q + D_{n-1}^q) + 9e^{(\frac{9}{4}\beta D_B)}(E_{n-1}^q + F_{n-1}^q) + e^{(\frac{1}{4}\beta D_B)}(G_{n-1}^q + 1)\,, \tag{15}$$

$$Q_B^0 = 4e^{(\frac{49}{4}\beta D_B)}(A_{n-1}^q + B_{n-1}^q) + 4e^{(\frac{25}{4}\beta D_B)}(C_{n-1}^q + D_{n-1}^q) + 4e^{(\frac{9}{4}\beta D_B)}(E_{n-1}^q + F_{n-1}^q) + 4e^{(\frac{1}{4}\beta D_B)}(G_{n-1}^q + 1)\,. \tag{16}$$

In order to calculate the compensation temperature, one has to define the global magnetization M_{net} of the model which is given by

$$M_{\text{net}} = \frac{M_A + M_B}{2}\,. \tag{17}$$

3. Definition of the Critical Temperatures

The most common phase transitions are of second-order or first-order type for all kinds of systems.

The Curie temperature or second-order transitions temperature T_c is the temperature at which both sublattice magnetizations and the global magnetization cancel continuously. T_c separates the ordered ferrimagnetic phase (F) from the disordered paramagnetic phase (P). At the Curie temperature, one can obtain the explicit expressions of the recursion relations given by:

For the spin-1 as

$$Y_n = Z_n = \frac{Y_1}{Y_0}\,, \tag{18}$$

where

$$Y_1 = e^{\frac{49D_B}{4}}\cosh\left(\frac{7\beta J}{2}\right)A_{n-1}^{q-1} + e^{\frac{25D_B}{4}}\cosh\left(\frac{5\beta J}{2}\right)C_{n-1}^{q-1} + e^{\frac{9D_B}{4}}\cosh\left(\frac{3\beta J}{2}\right)E_{n-1}^{q-1} + e^{\frac{D_B}{4}}\cosh\left(\frac{\beta J}{2}\right)G_{n-1}^{q-1}\,,$$

$$Y_0 = 2\left(e^{\frac{49D_B}{4}}A_{n-1}^{q-1} + e^{\frac{25D_B}{4}}C_{n-1}^{q-1} + e^{\frac{9D_B}{4}}E_{n-1}^{q-1} + e^{\frac{D_B}{4}}G_{n-1}^{q-1}\right)$$

and for the spin-7/2 as:

$$A_{n-1} = B_{n-1} = \frac{e^{D_A}\cosh\left(\frac{7\beta J}{2}\right)Y_n^{q-1} + 1}{e^{D_A}\cosh\left(\frac{\beta J}{2}\right)Y_n^{q-1} + 1}\,, \tag{19}$$

$$C_{n-1} = D_{n-1} = \frac{e^{D_A}\cosh\left(\frac{5\beta J}{2}\right)Y_n^{q-1}+1}{e^{D_A}\cosh\left(\frac{\beta J}{2}\right)Y_n^{q-1}+1}\,, \tag{20}$$

$$E_{n-1} = F_{n-1} = \frac{e^{D_A}\cosh\left(\frac{3\beta J}{2}\right)Y_n^{q-1}+1}{e^{D_A}\cosh\left(\frac{\beta J}{2}\right)Y_n^{q-1}+1}\,. \tag{21}$$

In addition to the thermal variations of the order-parameters and the global magnetization of the model, we also need to calculate and analyze the free-energy F' of the model in order to identify the first-order transitions temperature T_t. So, using the definition of the free-energy $F' = -kT\log(Z)$ in the thermodynamic limit as $(n \longrightarrow \infty)$ we expicitly obtain in terms of recursion relations as it is done in Refs. 39 and 40:

$$\begin{aligned}
F'/J = &-\frac{1}{\beta}\left\{\frac{q-1}{2-q}\ln[e^{\beta(\frac{-J}{2}+D_A)}Y_n^{q-1}+e^{\beta(\frac{J}{2}+D_A)}Z_n^{q-1}+1]\right\}\\
&-\frac{1}{\beta}\{\ln[e^{\beta(D_A)}Y_n^{q-1}+e^{\beta(D_A-)}Z_n^{q-1}+1]\}\\
&-\frac{1}{\beta}\left\{\frac{1}{2-q}\ln[e^{\beta(\frac{49D_B}{4}-)}A_{n-1}^{q-1}-+e^{\beta(\frac{49D_B}{4})}B_{n-1}^{q-1}\right.\\
&+e^{\beta(\frac{25D_B}{4})}C_{n-1}^{q-1}-+e^{\beta(\frac{25D_B}{4})}D_{n-1}^{q-1}\\
&+e^{\beta(\frac{9D_B}{4})}E_{n-1}^{q-1}-+e^{\beta(\frac{9D_B}{4})}F_{n-1}^{q-1}\\
&\left.+\ e^{\beta(\frac{D_B}{4})}G_{n-1}^{q-1}+e^{\beta(\frac{D_B}{4})}]\right\}\,.
\end{aligned} \tag{22}$$

We also investigate the compensation temperature $T_{\rm comp}$ at which the global magnetization cancels while both of the sublattice magnetizations do not cancel. $T_{\rm comp}$ is found by locating the crossing point of sublattice magnetizations curves i.e.,

$$M_A(T_{\rm comp}) = -M_B(T_{\rm comp})\,. \tag{23}$$

By making use of the different definitions of the critical temperatures, we are now ready to study the thermal variations of the calculated thermodynamical quantities and display the temperature phase diagrams of the model on all planes of interest.

4. Numerical Results and Discussions

In this section, we present and discuss the results we obtained for the thermal behaviors of the order-parameters and the temperature phase diagrams of the model. For this, we start discussions of the phase diagram at $T = 0$ which is very useful for the understanding of the obtained temperature phase diagrams.

4.1. *Ground-state phase diagram*

Before proceeding to the discussions of the numerical results for the temperature-dependence of the magnetic properties of the model, we analytically investigate first the ground-state phase diagram. The ground-state structure of the model can be found by comparing the values of the energy E_0 for different spin configurations. E_0 may be written as

$$E_0 = s\sigma - \frac{1}{q|J|}(D_A s^2 + D_B \sigma^2)\,. \tag{24}$$

Because of the ferrimagnetic coupling J, we only find six possible pairs of spins namely $O_1(\pm 1, \mp(7/2), 1, 49/4)$, $O_2(\pm 1, \mp(5/2), 1, 25/4)$, $O_3(\pm 1, \mp(3/2), 1, 9/4)$, $O_4(\pm 1, \mp(1/2), 1, 1/4)$, $D_1(0, 0, 0, 49/4)$ and $D_2(0, 0, 0, 1/4)$. Computational analysis of the corresponding energies in the reduced crystal-fields plane ($D_A/q|J|$ and $D_B/q|J|$) yields the phase diagram displayed in Fig. 2. The energies and the conditions for the occurence of the six possible states are shown in Table 1. This diagram shows some key features, in particular, the existence of four points (A, B, C and D) and coexistence lines where the spin pair energy of some phases coincides. For a given value of q and for $D_A/|J| \geq -(q/2)$, along the $D_B/q|J|$-axis, seven saturation values exist for M_B whereas for M_A, ± 1 is the only one value. Thus, we get the thermodynamic phases O_1, O_2, O_3 and O_4 and at the borders of these phases, three hybrid phases: $(\pm 1, \mp 3, 1, 9)$, $(\pm 1, \mp 2, 1, 4)$ and $(\pm 1, \mp 1, 1, 1)$ at the coexistence lines $D_B/|J| = -(4q/25)$, $D_B/|J| = -(q/4)$ and

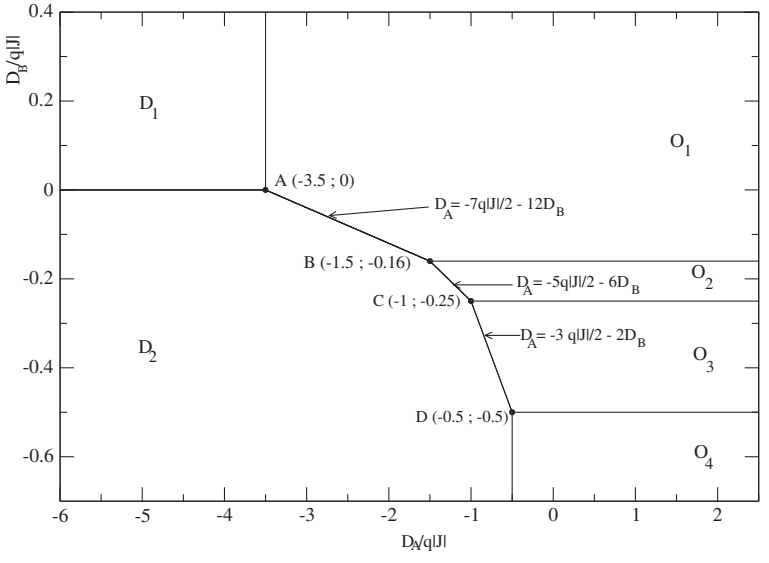

Fig. 2. Ground-state phase diagram of the mixed spin-1 and spin-7/2 Ising ferrimagnetic model with two different single-ion anisotropies D_A and D_B. Four-ordered phases (O_1, O_2, O_3 and O_4) and two particular disordered phases (D_1 and D_2) exist. At the coexistence lines, three hybrid phases may prevail (see text).

Table 1. Energies and conditions for the occurrence of the six spin configurations at the ground-state phase diagram for mixed spin-1 and spin-7/2 ferrimagnetic Ising model.

Spin configuration	Ground-state energy per site (E_0) of the state	Conditions for occurence
$D_1\left(0,0,0,\frac{49}{4}\right)$	$-\frac{49D_B}{8}$	$D_A \leq -\frac{7qJ}{2}$, $D_B \geq 0$
$D_1\left(0,0,0,\frac{1}{4}\right)$	$-\frac{1D_B}{8}$	$D_A \leq -\frac{7qJ}{2} - 12D_B$, $D_A \leq -\frac{5qJ}{2} - 6D_B$, $D_A \leq -\frac{3qJ}{2} - 2D_B$,$D_A \geq \frac{qJ}{4}$
$O_1\left(\pm 1,\mp\frac{7}{2},1,\frac{49}{4}\right)$	$-\frac{7qJ}{4} - \frac{D_A}{2} - \frac{49D_B}{8}$	$D_A \geq -\frac{7qJ}{2}$, $D_A \geq -\frac{7qJ}{2} - 12D_B$, $D_A \geq -\frac{qJ}{6}$
$O_2\left(\pm 1,\mp\frac{5}{2},1,\frac{25}{4}\right)$	$-\frac{5qJ}{4} - \frac{D_A}{2} - \frac{25D_B}{8}$	$D_A \geq -\frac{5qJ}{2} - 6D_B$, $-\frac{qJ}{4} \leq D_B \leq -\frac{qJ}{6}$
$O_3\left(\pm 1,\mp\frac{3}{2},1,\frac{9}{4}\right)$	$-\frac{3qJ}{4} - \frac{D_A}{2} - \frac{9D_B}{8}$	$-\frac{qJ}{2} \leq D_B \leq -\frac{qJ}{6}$, $D_A \geq -\frac{3qJ}{2} - 2D_B$
$O_4\left(\pm 1,\mp\frac{1}{2},1,\frac{1}{4}\right)$	$-\frac{qJ}{4} - \frac{D_A}{2} - \frac{D_B}{8}$	$D_B \geq -\frac{qJ}{2}$, $D_A \leq \frac{qJ}{4}$

$D_B/|J| = -(q/2)$ respectively. These hybrid phases should correspond to the cases where the sublattice B is half-half covered by spins of the two neighboring phases. It is worthwhile to mention that the diagram also shows two particular disordered phases D_1 and D_2. For the phase D_1 for example, $M_A = 0$ and one half of the sublattice B is covered by spin in state $7/2$ whereas the other half is covered by spin in state $-(7/2)$, so $M_B = 0$. Similar structure is observed for the disordered phase D_2. We also note that the disordered phases $(0,0,0,(25/4))$ and $(0,0,0,(9/4))$ are not found during our investigation. Indeed, by comparing different values of E_0 for the different spin configurations, for $D_B < 0$, the disordered phase D_2 may prevail whereas for $D_B > 0$, the disordered phase D_1 is more favorable. It is important to indicate that the ground-state phase diagram is very useful because it helps to check the reliability of the theoretical results and to classify the different phase regions of the model for the phase diagrams at higher temperatures.

4.2. *Thermal variations of the order-parameters*

As it is explained previously, the thermal variations of the order-parameters for the present model were obtained in terms of recursion relations. The thermal behaviors of the order-parameters play a crucial role in obtaining the finite-temperature phase diagrams of the system: When the magnetization curves go to zero continuously separating the ferrimagnetic phase from the paramagnetic phase, is the second-order phase transition or Curie temperature, i.e., the temperature at which magnetizations become zero. In the case of jumps in the magnetization curves followed by a discontinuity of the first derivative of the free-energy F', one gets a first-order

transition temperature. Besides these two critical temperatures, there is another temperature called compensation temperature defined as the temperature where the global magnetization becomes zero before the critical temperature. Therefore, in order to identify the second-order and first-order transition lines and the compensation lines, one has to study the thermal behaviors of the order-parameters. Now, we can present some results concerning the thermal behaviors of the order-parameters.

Figure 3 illustrates some thermal variations of the sublattice magnetizations M_1 and $M_{7/2}$ when $q = 3$. In panel (a), we have depicted the thermal behaviors of sublattice magnetizations M_1 at $M_{7/2}$ as functions of the temperature for selected values of $D_B/|J|$ when $D_A/|J| = 1$. The results are in perfect agreement with the ground-state phase diagrams concerning the saturation values. Indeed, M_1 falls from its unique saturation value ± 1 with increasing temperature whereas $M_{7/2}$ shows seven saturation values. For other values of the coordination q, the behaviors of the sublattice magnetizations M_1 and $M_{7/2}$ are quite similar. The Curie temperature T_c at which both magnetization curves go to zero increases with $D_B/|J|$. In panel (b), we have represented typical sublattice magnetizations M_1 and $M_{7/2}$ curves for four different values of $D_A/|J|$ when $D_B/|J| = 1$. From this panel, one can observe that both sublattice magnetizations show a unique saturation value and this is in perfect agreement with the ground-state phase diagram. Also, we note that all the curves are continuous and the Curie temperature T_c at which the two magnetization curves go to zero increases when $D_A/|J|$ increases.

Figure 4 expresses also some interesting thermal behaviors of the order-parameters for two values of the coordination number. From panels (a) to (d), we have displayed results of the thermal variations of the four considered order-parameters when $q = 3$. In panel (a), by setting $D_A = D_B = 3$, one can remark that the model shows only a second-order transition. Indeed from this panel, the sublattice magnetizations M_1 and $M_{7/2}$ fall respectively from their saturation values ± 1 and $\mp(7/2)$, decrease as the temperature increases and simultaneously go to zero at the Curie temperature T_c. The quadrupolar moments Q_1 and $Q_{7/2}$ fall also from their saturation values 1 and $49/4$ respectively and show little kinks at T_c. The second panel, i.e., panel (b) obtained for $D_B = 0$ and $D_A = 8.4$ shows that the model exhibits only first-order transitions at T_t where all the order-parameters present jump discontinuities. In panel (c) displayed for $D_A = -3$ and $D_B = -0.65$, we note that the system shows both first-order and second-order transitions. The panel (d) obtained for $D_A = 0$ and $D_B = -1.499$ shows that the order-parameters present similar thermal behaviors to those obtained in panel (a). The interesting result here concerned is, the thermal variations of the global magnetization M_{net} of the system as a function of the temperatures shown in the inset (i) of panel (d). The global magnetization cancels twice before going to the Curie temperature T_c. Here, the two compensation temperatures are respectively $T_{\text{comp}_1}/|J| \simeq 0.42$ and $T_{\text{comp}_2}/|J| \simeq 1.01$. This indicates that the model shows one or two compensation temperatures. Our result concerning the existence of the compensation tempera-

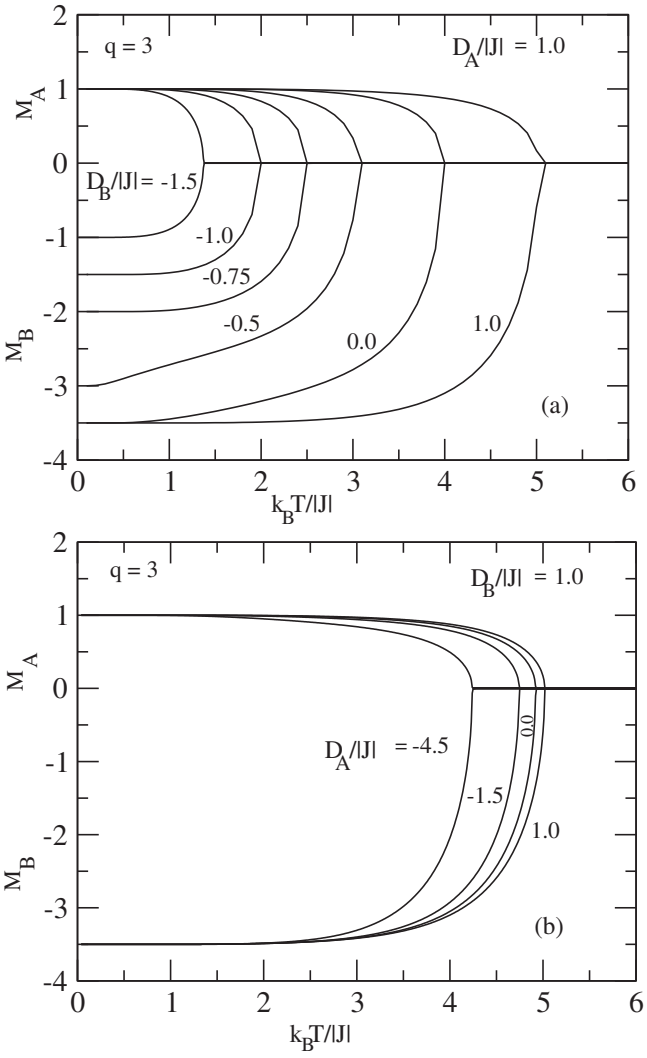

Fig. 3. Sublattice magnetizations of the model as functions of the reduced temperature $kT/|J|$ when $q = 3$ for various values of the crystal-fields interactions. Panel (a): Curves are displayed for $D_A/|J| = 1.0$ and selected values of $D_B/|J|$ indicated on the curves. Panel (b): Curves are displayed for $D_B/|J| = 1.0$ and selected values of $D_A/|J|$ indicated on the curves.

tures is in perfect agreement with Ref. 38 where the same model is studied. By means of standard MC simulations with the usual Metropolis algorithm[41] on a relatively small system of 32×32 lattice sizes with periodic boundary conditions, the previous results have been checked for $q = 4$, $D_A = 0$ and $D_B = -1.992$. A number of $5 \cdot 10^5$ MC steps and 6 independent runs are preformed. Physical quantities of interest are calculated after the system reaches a thermal equilibrium at the considered temperature. As indicated in the inset (ii) of panel (d), two compen-

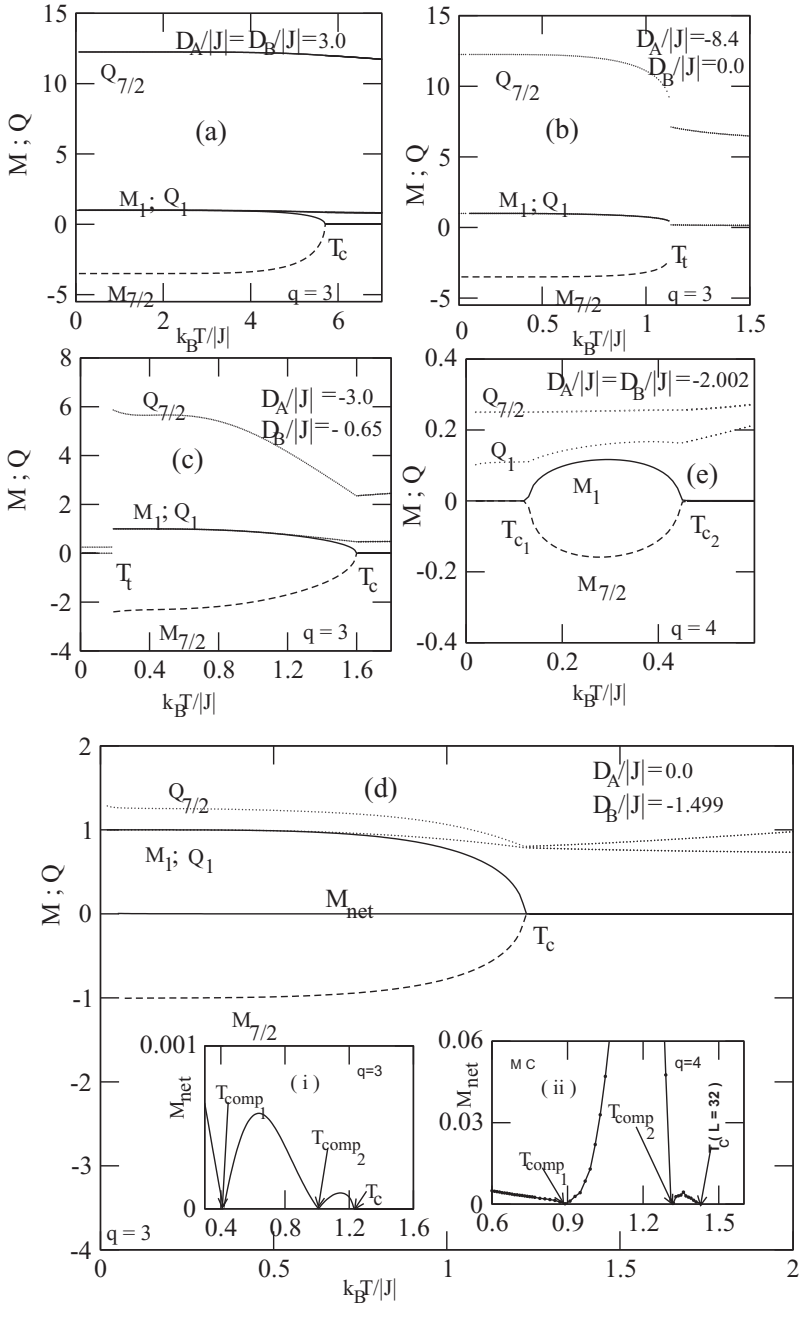

Fig. 4. Thermal variations of sublattice magnetizations and corresponding quadrupolar moments are calculated for $q = 3$ and 4 and for various values of the reduced crystal-fields as shown in the figures from panel (a) to panel (e). T_c, T_t and $T_{\rm comp}$ indicate respectively the second-order, first-order and compensation temperatures. Values of the physical parameters considered for the system are indicated in different panels.

sation points are also recovered. Extensive simulations and larger system sizes are certainly needed to get more accurate quantitative results. Since the BL approach neglects spin correlations that are important close to the Curie temperature, one may not expect to get quantitative agreement with results displayed in the inset (i). The last panel, where the calculations are made for $D_A = D_B = -2.002$ and $q = 4$, shows that the present model can exhibit also two Curie temperatures T_{c_1} and T_{c_2} respectively where the quadrupolar moments present little kinks. Figure 4 presents some similarities with Fig. 2 of Ref. 37.

To show how the crystal-fields affect the thermal behaviors of the global magnetization, we have displayed in Fig. 5, the thermal behaviors of the global magnetization for selected values of the crystal-fields when $q = 3$. We have only illustrated the case $q = 3$ due to similarities with other cases. We used the extended Néel classification[42,43] to refer to different types temperature-dependence of the global magnetization. The thermal variations of the global magnetization has been found to be of R-, S-, Q- and P-type.

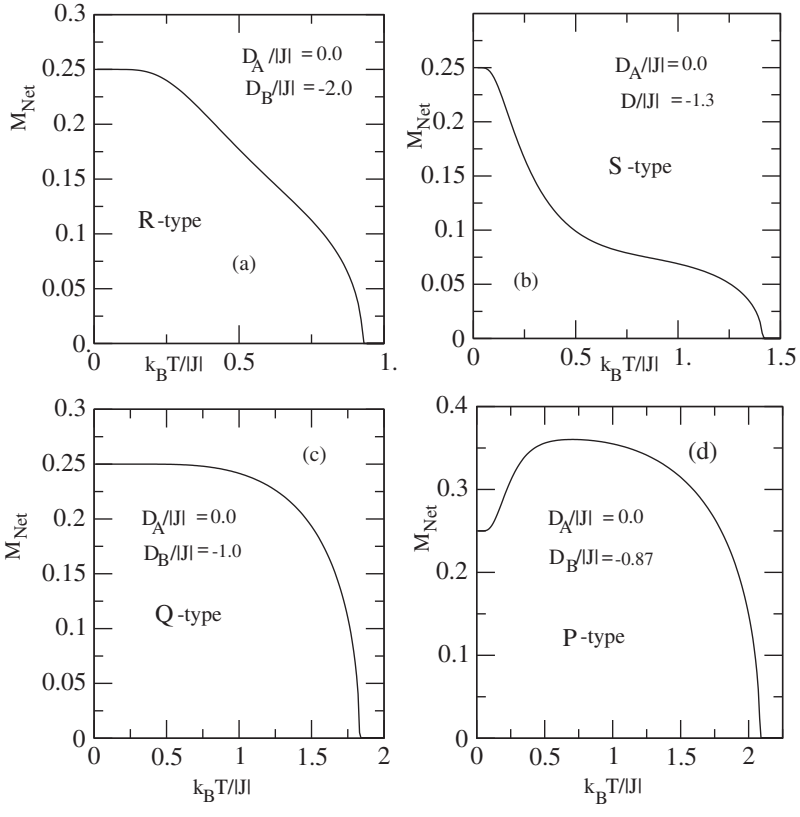

Fig. 5. Thermal variations of the global magnetization of the model for $q = 3$. Values of the physical parameters considered for the system are indicated in different panels.

4.3. *Finite-temperature phase diagrams*

After all the calculations, we can illustrate the temperature phase diagrams of the model. First, we have displayed the phase diagrams for $D_A = D_B = D$ on the $(D/|J|, kT/|J|)$ planes when $q = 3, 4$ and 6 (Fig. 6). Second, the finite-temperature

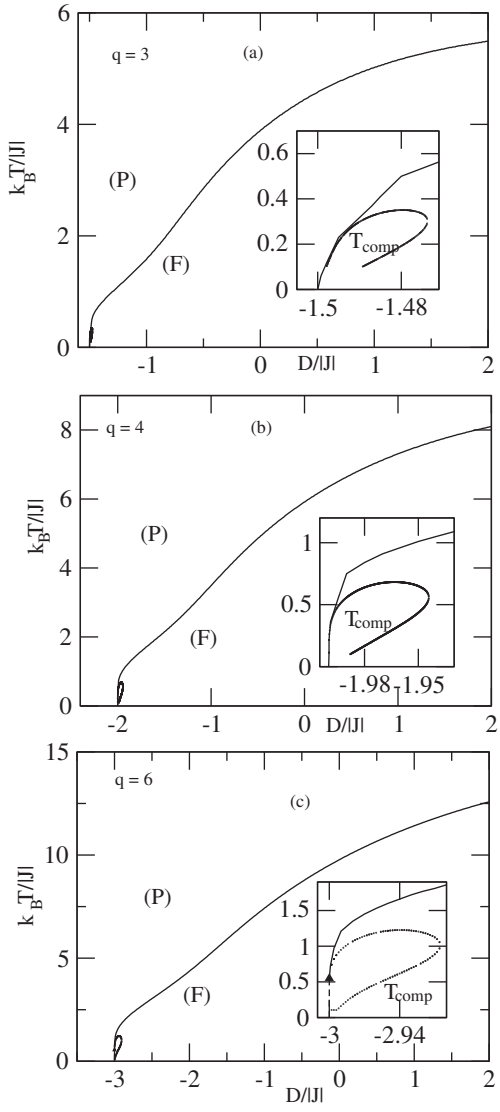

Fig. 6. Temperature phase diagrams for $D_A = D_B = D$ and $q = 3, 4$ and 6 in the $(D/|J|$ and $kT/|J|)$ planes. The solid, dashed, dotted lines and filled triangles indicate respectively the second-order transition line, the first-order transition line, the compensation line and the tricritical points. Panel (a): $q = 3$; panel (b): $q = 4$ and panel (c): $q = 6$. Here, the model presents tricritical behaviors in the case $q = 6$ and compensation lines are unclosed loops for all values of q.

phase diagrams are obtained respectively on the ($D_A/|J|$ and $kT/|J|$) plane for selected values of $D_B/|J|$ (Fig. 7) and on the ($D_B/|J|$ and $kT/|J|$) plane for selected values of $D_A/|J|$ (Figs. 8 and 9) when $q = 3$.

The first phase diagrams obtained on the ($D/|J|$ and $kT/|J|$) planes are displayed in Fig. 6. From this figure, some interesting properties of the system are singled out. Indeed for all value of the coordination number q, the compensation lines are unclosed loops which are obtained by the collection of the compensation temperatures. The transition lines are only of the second-order, separate the ferrimagnetic phase (F) from the paramagnetic phase (P) and go to the zero temperature at $D/|J| = -(q/2)$ when $q = 3$ or 4. For $q = 6$, the model shows a tricritical point located by ($D/|J| \simeq -2.99$, $kT/|J| \simeq 0.55$) and the first-order transition line existing at very low temperatures goes also to zero temperature at $D/|J| = -(q/2)$. It is important to indicate that the Curie temperature at which the second-order transition occurs increases with the coordination number q.

In Fig. 7, the phase diagram is given at fixed values of $D_B/|J|$ and varying values of $D_A/|J|$. When $D_B/|J| > 0$, all transition lines are of the second-order transition. All of them go to the zero temperature at the value $D_A/|J| = -(7q/2)$. On the ground-state phase diagram in Fig. 2, this value of $D_A/|J|$ lies in the boundary between the ordered phase O_1 and the disordered phase D_1. For $-(q/2) <$

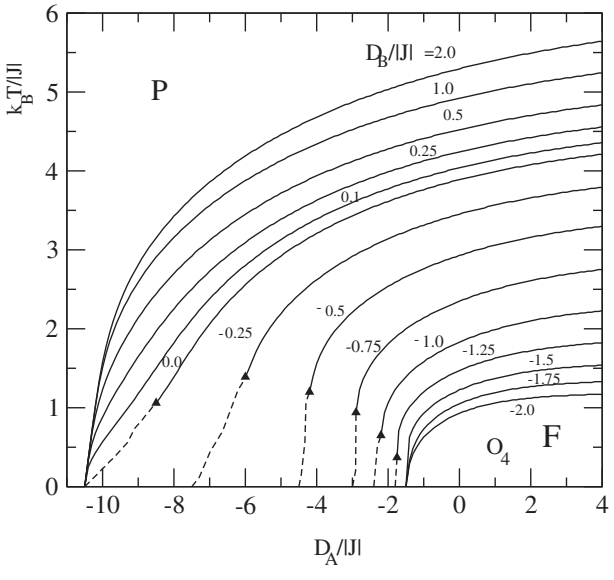

Fig. 7. Temperature phase diagram in the ($D_A/|J|$ and $k_BT/|J|$) plane at fixed values of $D_B/|J|$ is only illustrated for $q = 3$ due to the similarities with other cases. The solid, dashed, dotted lines and filled triangles indicate respectively the second-order transition line, the first-order transition line, the compensation line and the tricritical points. For $D_B/|J| > 0$ and $D_B/|J| \leq -(q/2)$, all the transition lines are of second-order. For other values of $D_B/|J|$, the model shows tricritical behaviors which means the existence of tricritical points.

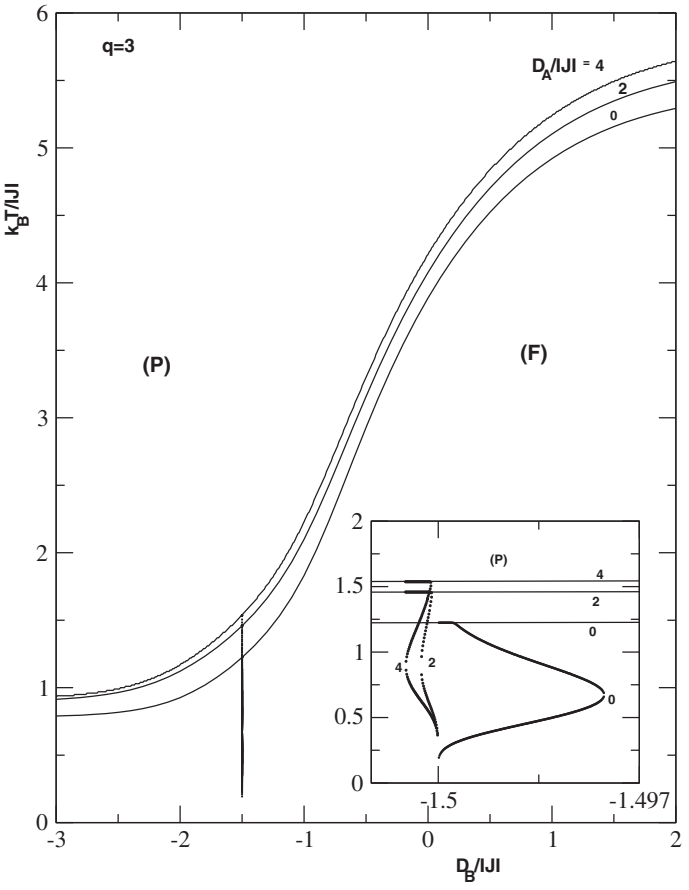

Fig. 8. Temperature phase diagram in the ($D_B/|J|$ and $k_BT/|J|$) plane at fixed values of $D_A/|J|$ illustrated only for $q = 3$ due to the presence of similarities with other cases when $D_A/|J| \geq 0$. The solid, dashed, dotted lines and filled triangles indicate respectively the second-order transition line, the first-order transition line, the compensation line and the tricritical points.

$D_B/|J| \leq 0$, the model shows tricritical behaviors which means that in this domain, the second-order transition line is connected to the first-order transition line at tricritical point. Indeed, when $-(4q/25) \leq D_B/|J| \leq 0$, the first-order transition line goes to zero temperature at a value of $D_A/|J|$ corresponding to $D_A/|J| = -12D_B/|J| - (7q/2)$, which also lies on the boundary of the phases O_1 and D_2 in the ground-state phase diagram. When $-(q/4) \leq D_B/|J| \leq -(4q/25)$, the first-order transition line goes to zero temperature at a value of $D_A/|J|$ corresponding to $D_A/|J| = -6D_B/|J| - (5q/2)$, which again lies on the boundary of the phases O_2 and D_2 in the ground-state phase diagram. When $-(q/2) < D_B/|J| \leq -(q/4)$, the first-order transition goes to zero temperature at a value of $D_A/|J|$ corresponding to $D_A/|J| = -2D_B/|J| - (3q/2)$, which is on the boundary of the phases O_3 and D_2 in the ground-state phase diagram. Finally, when $D_B/|J| \leq -(q/2)$, the

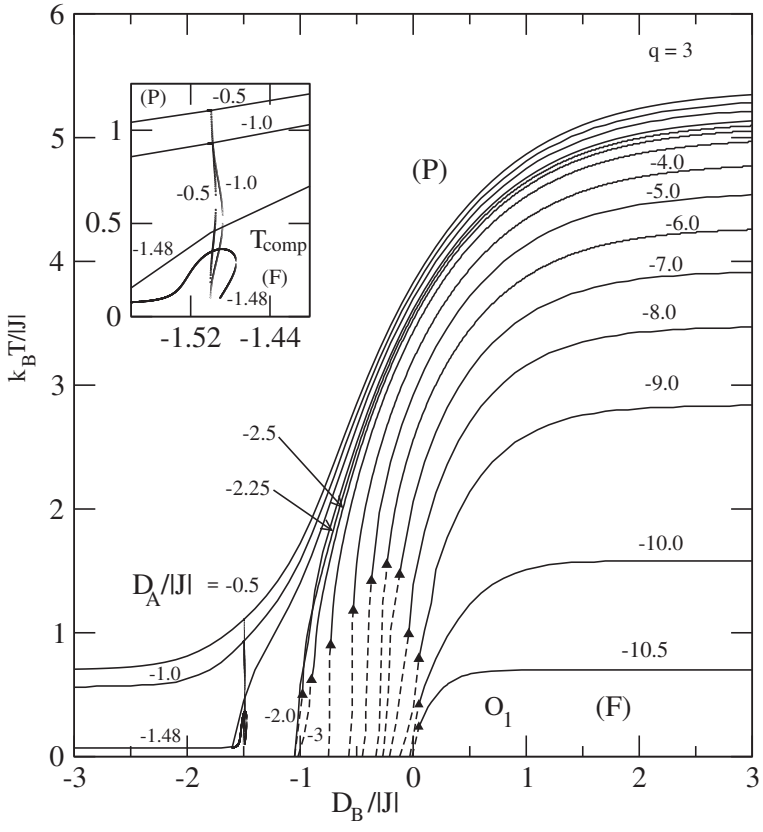

Fig. 9. Temperature phase diagram in the ($D_B/|J|$ and $k_BT/|J|$) plane at fixed values of $D_A/|J|$ illustrated only for $q = 3$ due to the presence of similarities with other cases when $D_A/|J| < 0$. The solid, dashed, dotted lines and filled triangles indicate respectively the second-order transition line, the first-order transition line, the compensation line and the tricritical points.

system exhibits only second-order transition and all the transition lines go to zero temperature at a same value of $D_A/|J| = -(q/2)$ which is also on the ground-state phase diagram, the boundary between the ordered phase O_4 and the disordered phase D_2. Such behaviors concerning the transition lines have been observed in Ref. 37.

The last phase diagrams are displayed for selected values of $D_A/|J|$ and varying values of $D_B/|J|$ as shown in Figs. 8–9. From these figures, one can observe that for $D_A/|J| \geq -(37q/75)$, the model exhibits only second-order transition and all the transition lines are constant at low temperature. Also, one can note that the model shows compensation points. For $-(2q/3) \leq D_A/|J| < -(37q/75)$, the system exhibits only second-order transition. For $-(7q/2) \leq D_A/|J| < -(2q/3)$, the model presents tricritical behaviors which means that the second-order transition line is connected to first-order transition line at tricritical point.

5. Conclusion

In this paper, we have studied the molecular magnetism of the mixed spin-1 and spin-7/2 BC Ising ferrimagnetic model on the BL by means of exact recursion equations method. All the thermodynamical functions of interest are obtained in terms of recursion equations.

The ground-state phase diagram of the model was constructed as shown in Fig. 2. In this phase diagram, we have found four-ordered phases (O_1, O_2, O_3, O_4), two particular disordered phases (D_1, D_2) and three hybrid phases near the coexistence lines. This ground-state phase diagram is used as a guide in obtaining the different temperature phase diagrams. We also investigated the thermal variations of the sublattice magnetizations, the corresponding quadrupolar moments and the global magnetization of the model which are shown in Figs. 3–5. From these figures, the order-parameters showed in most cases, the usual decay with thermal fluctuations. By using the thermal behaviors of the considered order-parameters and the analysis of the free-energy, the nature of the different phase transitions encountered is identified. This enables us to present and discuss in detail the different finite-temperature phase diagrams in the cases of equal and unequal crystal-fields interactions as shown in Figs. 6–9. We have found that the model presents very rich critical behaviors, which include first-order and second-order transitions as well as tricritical points in the physical parameters' space. We have also found that the model displays the compensation phenomenon where the compensation points were identified for appropriate values of the crystal-fields interactions.

Finally, we should mention that the different results achieved here bear some topological resemblances with those reported in Refs. 37 and 38.

References

1. R. M. White, *Science* **229**, 11 (1985).
2. R. Wood, *Understanding Magnetism* (Tab Books Inc, Blue Ridge Summit, PA, 1988).
3. E. Köster, *J. Magn. Magn. Mater.* **120**, 1 (1988).
4. L. B. Lueck and R. G. Gilson, *J. Magn. Magn. Mater.* **88**, 227 (1999).
5. K. Itoh and M. Kinoshita, *Molecular Magnetism: New Magnetic Materials* (Kodansha, Tokyo, 2000).
6. W. Linert and M. Verdaguer, *Molecular Magnets: Recent Highlights* (Springer, Berlin, 2003).
7. D. Gatteschi, *Advo. Matter.* **6**, 635 (1994).
8. J. S. Miller and A. J. Epstein, *Chem. Eng. News* **73**, 30 (1995).
9. O. Kahn, *Molecular Magnetism* (VCH, New York, 1993).
10. A. Bobák, *Physica A* **258**, 140 (1998).
11. T. Kaneyoshi, *J. Phys. Soc. Japan* **56**, 2675 (1987).
12. T. Kaneyoshi, *Physica A* **153**, 556 (1988).
13. T. Kaneyoshi, *J. Magn. Magn. Mater.* **92**, 59 (1990).
14. A. Benyoussef, A. El Kenz and T. Kaneyoshi, *J. Magn. Magn. Mater.* **131**, 173 (1994).
15. A. Benyoussef, A. El Kenz and T. Kaneyoshi, *J. Magn. Magn. Mater.* **131**, 179 (1994).
16. A. Bobák and M. Jurčišin, *Physica A* **240**, 647 (1997).
17. D. C. de Oliveira *et al.*, *Physica A* **386**, 205 (2007).

18. T. Kaneyoshi, M. Jurčišin and P. Tomczack, *J. Phys. Condens. Matter* **4**, L653 (1992).
19. T. Kaneyoshi, *Physica A* **205**, 677 (1994).
20. D. F. de Albuquerque, S. R. L. Alves and A. S. de Arruda, *Phys. Lett. A* **346**, 128 (2005).
21. H. K. Mohamad, E. P. Domashevskaya and A. F. Klinskikh, *Physica A* **388**, 4713 (2009).
22. T. Kaneyoshi and J. C. Chen, *J. Magn. Magn. Mater.* **98**, 201 (1991).
23. W. G. Zhu and M. H. Ling, *Commun. Theor. Phys.* **51**, 756 (2009).
24. S. G. A. Quadros and S. R. Salinas, *Physica A* **206**, 479 (1994).
25. G. M. Zhang and C. Z. Yang, *Phys. Rev. B* **48**, 9452 (1993).
26. G. M. Buendia and M. A. Novotny, *J. Phys.: Condens. Matter* **9**, 5951 (1997).
27. G. M. Buendia and J. A. Liendo, *J. Phys.: Condens. Matter.* **9**, 5439 (1997).
28. M. Godoy and W. Figueiredo, *Phys. Rev. E* **61**, 218 (2000).
29. M. Godoy and W. Figueiredo, *Phys. Rev. E* **65**, 026111 (2002).
30. M. Godoy and W. Figueiredo, *Phys. Rev. E* **66**, 036131 (2002).
31. G. Wei, Q. Zhang and Y. Gu, *J. Magn. Magn. Mater.* **301**, 245 (2006).
32. G. Wei, Y. Gu and J. Liu, *Phys. Rev. B* **74**, 024422 (2006).
33. M. Zukovič and A. Bobák, *Physica A* **389**, 5401 (2010).
34. M. Zukovič and A. Bobák, *J. Magn. Magn. Mater.* **322**, 2868 (2010).
35. R. A. Yessoufou, S. Bekhechi and F. Hontinfinde, *Eur. Phys. J. B* **81**, 137 (2011).
36. J. Kplé, R. A. Yessoufou and F. Hontinfinde, *Afr. Rev. Phys.* **7**, 139 (2012).
37. E. Albayrak and A. Yigit, *Chin. Phys. B* **21**, 020511 (2012).
38. H. K. Mohamad, *Int. J. Adv. Res.* **9**, 442 (2014).
39. E. Albayrak, *Int. J. Mod. Phys. B* **17**, 1087 (2008).
40. E. Albayrak and A. Yigit, *Phys. Lett. A* **353**, 121 (2006).
41. N. C. Metropolis *et al.*, *J. Chem. Phys.* **21**, 1087 (1953).
42. L. Néel, *Ann. Phys.* **3**, 137 (1948).
43. S. Chikazumi, *Physics of Ferromagnetism*, 2nd edn. (Oxford University Press, Oxford, 1997).